20th AIAA Computational Fluid Dynamics Conference
27 - 30 June 2011, Honolulu, Hawaii

AIAA 2011-3551

# A Computational Fluid Dynamics Analysis of a High-Pressure Photo-Emission Gas Spectrometer

**Axel Rohde[1] and Yongho Lee[2]**
*Department of Engineering Sciences*
*Embry-Riddle Aeronautical University*
*Daytona Beach, Florida 32114*

**A supersonic flow through a photo-emission gas spectrometer that consists of differentially pumped axisymmetric vacuum chambers is investigated in the present work. In order to capture the shock waves residing in the chambers due to high inlet-to-exit pressure ratios, the flux vector splitting technique of Van Leer was applied to the finite volume formulation of the Euler equations. A uniform Cartesian mesh was used to discretize the entire domain, both fluid and solid, and cut cells combined with a flow tangency condition were employed at the fluid-solid interface. At very high pressure ratios, a periodic motion of shock waves was observed in the chambers. For verification of the computed results, a comparison study was conducted with the use of a commercial CFD software, capable of performing dynamic grid adaptation.**

## Nomenclature

| | | |
|---|---|---|
| $a$ | = | speed of sound |
| $c_p$ | = | specific heat at constant pressure |
| $c_v$ | = | specific heat at constant volume |
| $dA$ | = | differential area |
| $dV$ | = | differential volume |
| $d$ | = | diameter |
| $e$ | = | internal energy per unit mass |
| $e_0$ | = | stagnation energy per unit mass |
| $\mathbf{F}$ | = | flux vector system |
| $\mathbf{F}^{\pm}$ | = | flux vector split system |
| $h$ | = | enthalpy per unit mass |
| $h_0$ | = | stagnation enthalpy per unit mass |
| $k_B$ | = | Boltzmann constant |
| $Kn$ | = | Knudsen number |
| $L$ | = | length |
| $M$ | = | Mach number |
| $\hat{n}$ | = | unit normal vector |
| $p$ | = | pressure |
| $\mathbf{Q}$ | = | flow vector system |
| $R$ | = | gas constant |
| $\mathbf{S}$ | = | source vector system |
| $t$ | = | time |
| $T$ | = | temperature |
| $u, v$ | = | Cartesian velocity components |
| $\vec{v}$ | = | velocity vector |
| $x, y$ | = | Cartesian coordinates |
| $\gamma$ | = | ratio of specific heats |
| $\lambda$ | = | mean free path length |
| $\rho$ | = | density |

**Subscripts**

| | | |
|---|---|---|
| 0 | = | high pressure chamber |
| 1 | = | first vacuum chamber |
| 2 | = | second vacuum chamber |
| $CS$ | = | control surface |
| $CV$ | = | control volume |
| $n$ | = | normal component |
| $x, y$ | = | Cartesian components |

**Superscripts**

| | | |
|---|---|---|
| $+$ | = | right-running flux |
| $\pm$ | = | right- / left-running flux |
| $-$ | = | left-running flux |

[1] Retired 15 May 2011, AIAA Senior Member.
[2] Associate Professor, AIAA Senior Member.

## I. Introduction

Traditionally, photo emission spectroscopy is used in the chemical surface analysis of solids, with the sample under investigation being placed in a high vacuum [1]. A monochromatic x-ray beam is focused on the sample which induces photo electric ionization [2]. The energies of the scattered photo electrons are characteristic of the chemical structure of the sample and can be measured by an electron analyzer or spectrometer. The surrounding vacuum assures that scattered photo electrons do not interact with gas molecules, which would alter their energy state and thus send a distorted signal to the spectrometer. The necessary presence of a vacuum, however, restricts the type of samples that can be analyzed to solids and high viscosity oils, since most liquids would simply evaporate before the testing could begin.

The prototype spectrometer developed by Berkeley National Laboratory manages to work around the vacuum condition, thus allowing the testing of a wider range of samples [3]. A schematic of Berkeley Laboratory's gas spectrometer is shown in Figure 1. The sample is placed in a high pressure chamber which operates in the hectopascal range. Within millimeters of the sample, a small aperture opens into a series of differentially pumped vacuum chambers, which are axially symmetric. As with a traditional spectrometer, an x-ray beam is focused on the sample which induces the desired photo electric effect. A small portion of the photo electrons scattered from the sample exits through the aperture into the vacuum chambers. These electrons are then collimated into a beam through an electrostatic lens system, comprised of the positively charged vacuum chambers, and the beam stays focused along the optical axis until it reaches the analyzer. Since the photo electrons exiting the aperture only interact with gas molecules at hectopascal pressure over a very short distance, signal distortion is minimized. Once within the vacuum chambers, the gas pressure quickly drops off into the centi- and millipascal range, and collisions between electrons and gas molecules become rare. The application range of such a gas spectrometer is virtually unlimited, since any type of sample can be analyzed for chemical surface composition.

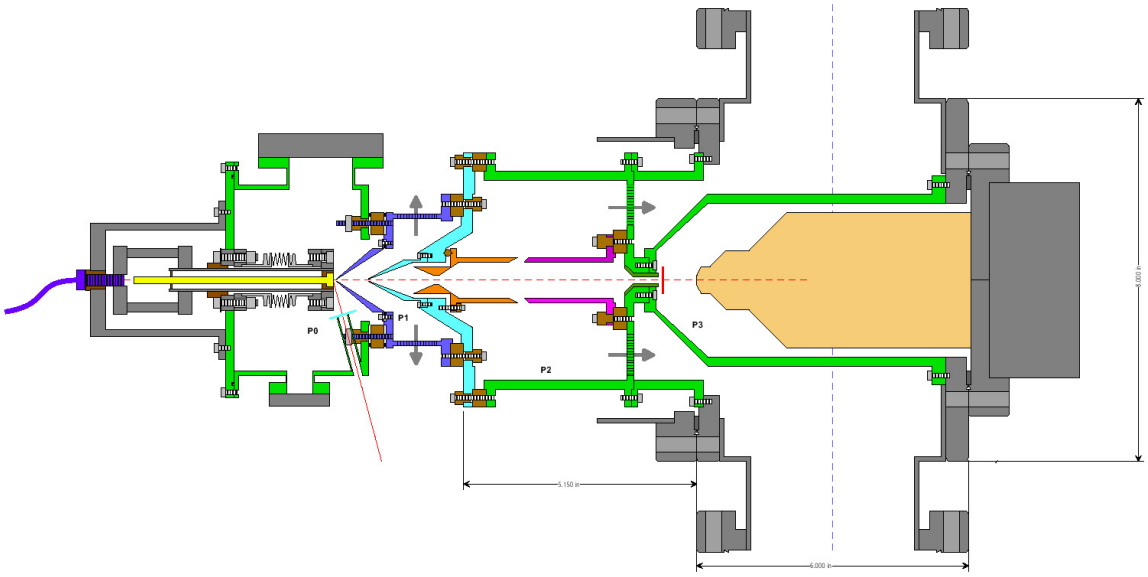


**Figure 1**: Photo Emission Gas Spectrometer – Courtesy of Berkeley National Laboratory

In order to improve and ultimately optimize the design of the photo emission gas spectrometer, one must precisely know the density variation of the gas along the optical axis from the sample to the electron analyzer. As the gas leaves the high pressure chamber, it expands and reaches locally supersonic flow speed, which can only be slowed down to subsonic speed through a shock before it enters the next chamber. This process is repeated through each vacuum chamber until the gas becomes so rarefied that the mean free path length of the gas molecules is comparable in size to the dimensions of the chambers. In this regime of free molecular flow, collision rates of gas molecules with themselves and with the photo electrons become vanishingly small, and the energy states of the electron beam are essentially preserved.

It should be noted that in the free molecular flow regime, the continuum hypothesis of the gas is no longer valid, which means that macroscopic quantities such as pressure, density and temperature at any given point in the flow can no longer be clearly defined. Up to that point, however, the flow properties along the optical axis can be predicted through a computational fluid dynamics (CFD) analysis by solving the flow field throughout all chambers subject to properly described flow conditions at their inlets and exits. Such a CFD simulation is the scope of this work.

## II. Analysis

The geometry of the physical model used for the flow analysis is shown in Figure 2, which represents a small section of the entire gas spectrometer outlined in Figure 1. The origin of the coordinate system of the solid model in Figure 2 is located at the inlet to the high pressure chamber, where a constant pressure of $p_0$ is prescribed (see also Figure 1). The $x$-axis is aligned with the optical axis and points along the direction of travel of the photo electron beam. The sample is located along the optical axis right before the aperture to the first vacuum chamber, but is omitted in the solid model in Figure 2. Air is pumped out of the first vacuum chamber in a radial manner, with the pressure at the cylindrical outflow boundary being kept at $p_1$. At the circular outflow boundary to the second vacuum chamber, the pressure is kept at a constant value of $p_2$. The pressure ratios between the high pressure chamber ($p_0$) and the two vacuum chambers ($p_1$, $p_2$) are on the order of $p_0/p_1$ = 1E+3 to 1E+4 and $p_0/p_2$ = 1E+4 to 1E+5, respectively. The aperture diameter of both vacuum chambers is 0.04 inch (1 mm). The overall dimensions of the model are $8 \times 8$ inches ($20 \times 20$ cm).

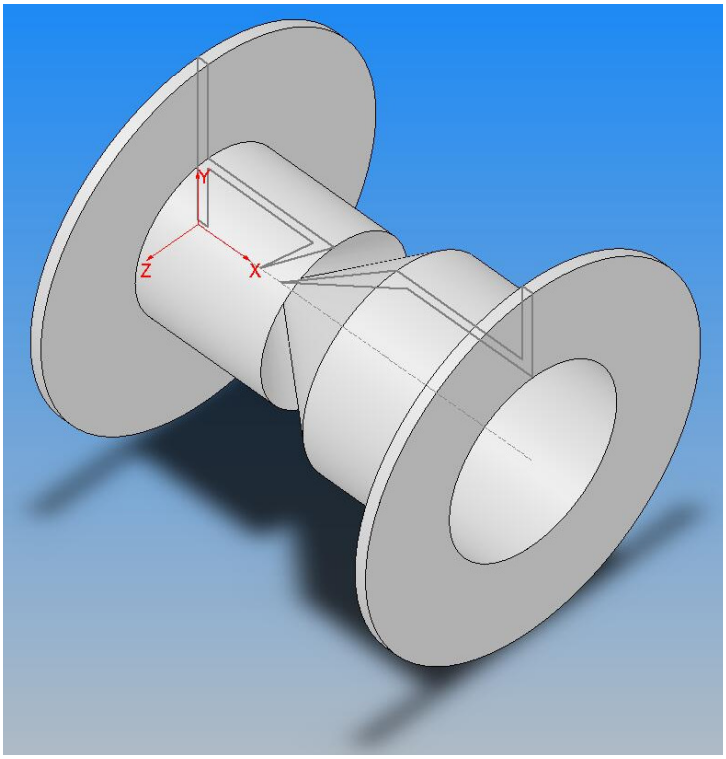


**Figure 2**: Solid Model of Pressure Chambers

Due to the large pressure drop across the spectrometer, the flow between the inlet and exit stagnation regions undergoes multiple supersonic expansions and shocks, which at times can even be unsteady. Therefore, a flow simulation based on computational fluid dynamics (CFD) must be able to capture and resolve shock waves with reasonable accuracy, especially in a time varying flow where shocks are moving. The present analysis uses Van Leer's flux vector splitting algorithm applied to a finite volume description of the unsteady Euler equations for shock capturing. The simulation was implemented by modifying the shareware *MicroCFD* Virtual Wind Tunnel, created and maintained by the first author of this paper [4].

The Euler equations describing the unsteady motion of inviscid axisymmetric flow can be written as a system of integral conservation equations for mass, momentum, and energy. In vector form, the equations are the sum of a volume and a surface integral, which is balanced by a source term in the radial momentum equation due to the asymmetric pressure that acts on a typical axisymmetric volume element,

$$\frac{\partial}{\partial t}\int_{CV} \mathbf{Q}\, dV \;+\; \oint_{CS} \mathbf{F}\, dA \;=\; \int_{CV} \mathbf{S}\, dV\,, \tag{1}$$

where **Q**, **F**, and **S** are column vectors given by

$$\mathbf{Q} = \begin{bmatrix} \rho \\ \rho u \\ \rho v \\ \rho e_0 \end{bmatrix}, \qquad \mathbf{F} = \begin{bmatrix} \rho v_n \\ \rho u v_n + p n_x \\ \rho v v_n + p n_y \\ \rho h_0 v_n \end{bmatrix}, \qquad \mathbf{S} = \begin{bmatrix} 0 \\ 0 \\ p/y \\ 0 \end{bmatrix}, \tag{2}$$

and the differential volume and area are

$$dV = y\, dx\, dy \qquad \text{and} \qquad dA = y\sqrt{(dx)^2 + (dy)^2}\,. \tag{3}$$

In the above equations, $\rho$ is the density, $p$ is the pressure, and $u$ and $v$ are the velocity components in the $x$ and $y$-direction respectively, with $x$ pointing along the symmetry axis and $y$ along the radial direction. Due to the Cartesian mesh used in the present analysis, the components of the outward normal on the cell surfaces, away from the solid boundaries, only vary between 0 and ±1. The velocity across a cell boundary, $v_n$, is defined as the dot product of local velocity vector and outward unit normal vector to the boundary,

$$v_n = \vec{v}\cdot\hat{n} = u\, n_x + v\, n_y\,. \tag{4}$$

When the body forces are neglected, the specific stagnation energy, $e_0$, includes only specific internal energy, $e$, and specific kinetic energy. Likewise, the specific stagnation enthalpy, $h_0$, is the sum of static ($h$) and dynamic parts, hence we have,

$$e_0 = e + \tfrac{1}{2}(u^2 + v^2) \qquad \text{and} \qquad h_0 = h + \tfrac{1}{2}(u^2 + v^2)\,. \tag{5}$$

For a thermally and calorically perfect gas, the static internal energy and enthalpy are only functions of temperature, $T$, or speed of sound, $a$,

$$e = c_v T = \frac{a^2}{\gamma(\gamma-1)} \qquad \text{and} \qquad h = c_p T = \frac{a^2}{\gamma-1}\,, \tag{6}$$

where the specific heats for constant volume and constant pressure processes, $c_v$ and $c_p$, as well as their ratio, $\gamma$, and their difference, $R$, are assumed to be constant,

$$\gamma = \frac{c_p}{c_v} \qquad \text{and} \qquad R = c_p - c_v\,. \tag{7}$$

Under the simplifying assumptions mentioned above, the speed of sound is a function of temperature only, and the pressure, density, and temperature are related by the ideal gas state equation,

$$a = \sqrt{\gamma R T} \qquad \text{and} \qquad p = \rho R T\,. \tag{8}$$

With these constitutive relations, the system of integral conservation equations is now closed and has four equations with four unknowns for a given geometry: two velocity components and two thermodynamic state variables such as pressure and temperature.

For a given local Mach number, $M_n = v_n/a$, normal to a cell boundary, the flow vector (**Q**) and flux vector (**F**) are written in the following format, after expressing energy, enthalpy, and pressure in terms of the local speed of sound:

$$\mathbf{Q} = \rho \begin{bmatrix} 1 \\ u \\ v \\ \dfrac{a^2}{\gamma(\gamma-1)} + \dfrac{u^2+v^2}{2} \end{bmatrix}, \qquad \mathbf{F} = \rho a \begin{bmatrix} M_n \\ u M_n + \dfrac{a}{\gamma} n_x \\ v M_n + \dfrac{a}{\gamma} n_y \\ \left( \dfrac{a^2}{\gamma-1} + \dfrac{u^2+v^2}{2} \right) M_n \end{bmatrix}. \tag{9}$$

Central difference type numerical schemes split the flux vector symmetrically into right and left running fluxes, $\mathbf{F}^+$ and $\mathbf{F}^-$. Such schemes do not take into consideration the direction of signal propagation within the flow field and cannot distinguish between subsonic and supersonic flow. As a result, shock waves are not properly resolved and spurious oscillations are common within the flow field, even for a purely subsonic flow. Based on an eigenvalue analysis of the Euler equations, Van Leer proposed an upwind scheme that splits the flux vector according to the locally characteristic directions [5]. Van Leer's scheme clearly separates subsonic flow from supersonic flow depending on the local Mach number such that $\mathbf{F} = \mathbf{F}^+ + \mathbf{F}^-$ for all values of $M_n$. If $M_n \le -1$, then $\mathbf{F}^+ = 0$ and $\mathbf{F}^- = \mathbf{F}$. If $M_n \ge +1$, then $\mathbf{F}^+ = \mathbf{F}$ and $\mathbf{F}^- = 0$. If $-1 < M_n < +1$, then

$$\mathbf{F}^{\pm} = \pm \frac{\rho a (M_n \pm 1)^2}{4} \begin{bmatrix} 1 \\ \dfrac{n_x(\pm 2a - v_n)}{\gamma} + u \\ \dfrac{n_y(\pm 2a - v_n)}{\gamma} + v \\ \dfrac{a^2}{\gamma-1} - \dfrac{(\pm a - v_n)^2}{\gamma+1} + \dfrac{u^2+v^2}{2} \end{bmatrix}. \tag{10}$$

The steady-state solution to the flow field is obtained by marching in time from an initial condition of uniform pressure and temperature ($p_0$, $T_0$) in all chambers, subject to three sets of boundary conditions: prescribed pressure and temperature at the inlet boundary, prescribed pressures at the exit boundaries, and tangential (slip) flow with zero energy flux at all solid surfaces. The velocity at the inlet and exit, as well as the temperature at all exits, develops naturally through a zero gradient (Neumann) boundary condition. The entire computational domain, both fluid and solid, is discretized on a Cartesian mesh of uniform spacing. At the fluid-solid interface cut cells are employed, such that the flow is tangent to the solid surface, consistent with the description of inviscid flow.

Due to the very low pressures in the vacuum chambers, which are in the centi- and millipascal range, the continuum hypothesis of the gas breaks down, and the flow may enter the free molecular regime. Macroscopic quantities such as pressure and temperature are no longer well defined at any point in a free molecular flow due to rare intermolecular collisions, and as a result the Euler and Navier Stokes equations are superseded by the Boltzmann equations [6]. A criterion which classifies a particular flow regime is the Knudsen number, $Kn = \lambda/L$, the ratio of the molecular mean free path length, $\lambda$, to a representative physical length, $L$. The distance of the mean free path is a function of temperature, pressure, and the diameter of the gas molecules, $d$. Combined with the Boltzmann constant, $k_B$, the Knudsen number can be evaluated as

$$Kn = \frac{k_B T}{p L \sqrt{2} \pi d^2}. \tag{11}$$

With $k_B$ = 1.38E–23 J/K, $T$ = 295 K, $L$ = 0.1 m, $d$ = 3.7E–10 m for an average air molecule diameter according to reference [7], and $p$ = 0.0133 Pa in the second vacuum chamber, a Knudsen number of $Kn$ = 5.0 is calculated. For $0.2 \le Kn \le 20$, a flow is considered to be in a transitional regime between continuum and free molecular flow [6].

Although the Euler equations are placed at the low end of the continuum flow spectrum, with $Kn < 0.01$, the Navier Stokes equations hold up to $Kn = 0.2$ if one allows a velocity slip condition at solid surfaces [8]. Due to the numerical viscosity present in the flux vector splitting algorithm, the Euler solver is comparable to a Navier Stokes solver modeling a slip condition and thus produces reliable results up to $Kn = 0.2$. Although the flow in both exit chambers is clearly in the transitional regime (for the first vacuum chamber, the exit pressure is 1/10 compared to the second chamber, and thus the Knudsen number is about 0.5), the results of the present analysis can still be considered a good first-order approximation. In order to model transitional flow more accurately, one would need to solve the Boltzmann equations through a direct simulation Monte Carlo method (DSMC). DSMC methods model gas flow through molecular collisions directly [9], and thus are even more computationally expensive, unless the flow is well within the free molecular regime [10]. Furthermore, Berkeley Lab intends to design gas spectrometers that run at higher pressures, such that the flow within the exit chambers will stay below the critical Knudsen number of 0.2.

## III. Results and Discussion

All computations shown in the present work were carried out for the $8 \times 4$ inch ($20 \times 10$ cm) axisymmetric geometry. As mentioned earlier, the entire computational domain, both fluid and solid, is discretized on a Cartesian mesh of uniform spacing. Cut cells are employed at the fluid-solid interface, such that the flow is tangent to the solid surface, consistent with the description of inviscid flow. Initially, $800 \times 400$ finite volume cells were used in the entire domain for all the computed cases, but later the mesh density was doubled in each direction to ensure grid-independence of the numerical solution. Unless otherwise noted, all the presented results are from the $1600 \times 800$ high-resolution simulations, corresponding to 1.28 million fluid and solid cells. After doubling the mesh density in both directions, the authors did not observe any noticeable difference in the flow structure and the quantitative comparison was also satisfactory; for example, the change in the maximum Mach number was approximately 12%. Although many cases were run during the overall investigation, with different geometries and a variety of gases, only two typical cases are presented here, which capture most of the physical phenomena observed.

Figure 3 exhibits the contour plot of Mach number at $p_0/p_1 = 1E+3$, $p_0/p_2 = 1E+4$, and $T_0 = 295$ K. The gas constant and the specific heat ratio of air used in the computations are $R = 287$ J/(kg·K) and $\gamma = 1.4$. The flow within the high pressure chamber is mostly stagnant and starts to accelerate in the proximity of the first aperture or *nozzle* due to the strong pressure gradient. At the smallest opening diameter or *nozzle throat* the flow reaches sonic speed (Mach 1) and thereafter accelerates to high supersonic speed (Mach 10) as it expands into the first vacuum chamber. In order to decelerate from supersonic to subsonic speed, a flow must undergo a strong compression or *shock* wave, well pronounced by a sudden decrease in Mach number, which is accompanied by an abrupt increase in pressure, density, and temperature.

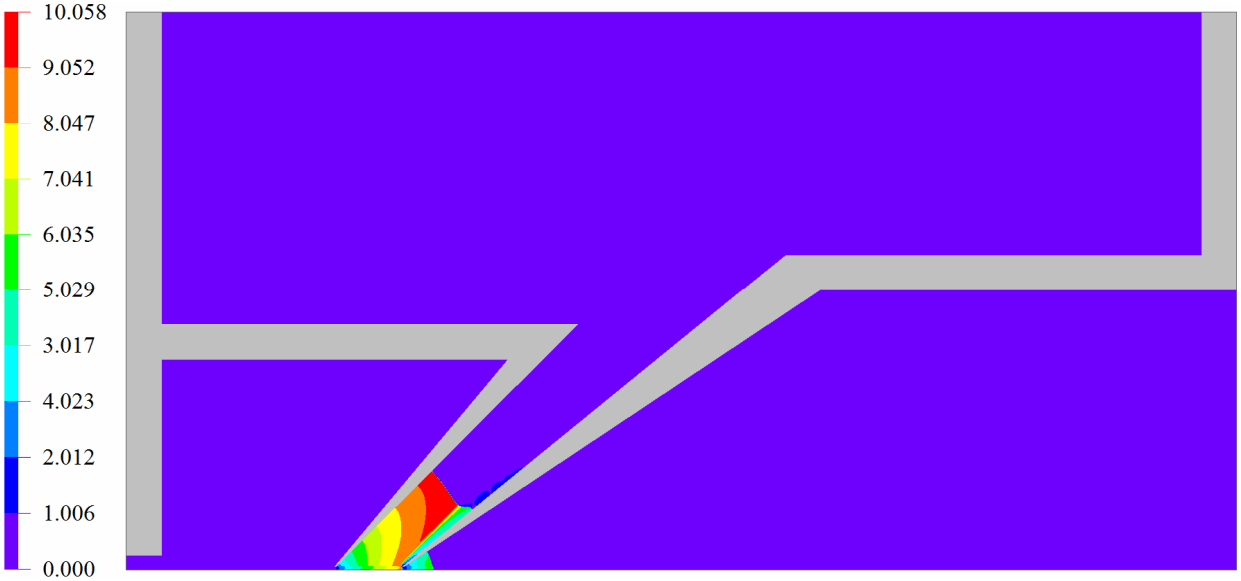


**Figure 3**: Mach number contours at lower inlet-to-exit pressure ratios

In Figure 4(a), which displays the magnified view of Mach number contours near the small openings, three shock waves can be identified. The first shock is positioned well above the optical axis within the first vacuum chamber. The second shock is located right in front of the opening to the second vacuum chamber, and it crosses the symmetry axis. The third shock is inside the second vacuum chamber and also crosses the symmetry or optical axis. The first shock is by far the strongest, since it has the largest reduction in Mach number. After the first and third shock have decelerated the flow to subsonic speed, the widening geometry in both vacuum chambers further slows down the exiting flow to Mach numbers approaching nearly zero.

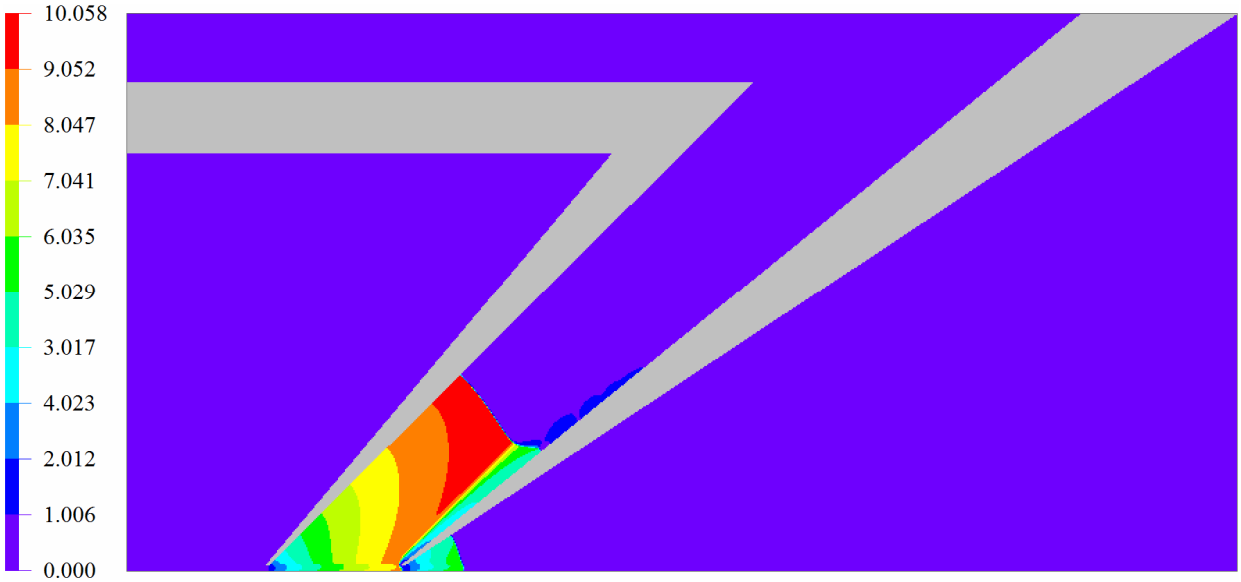


(a)

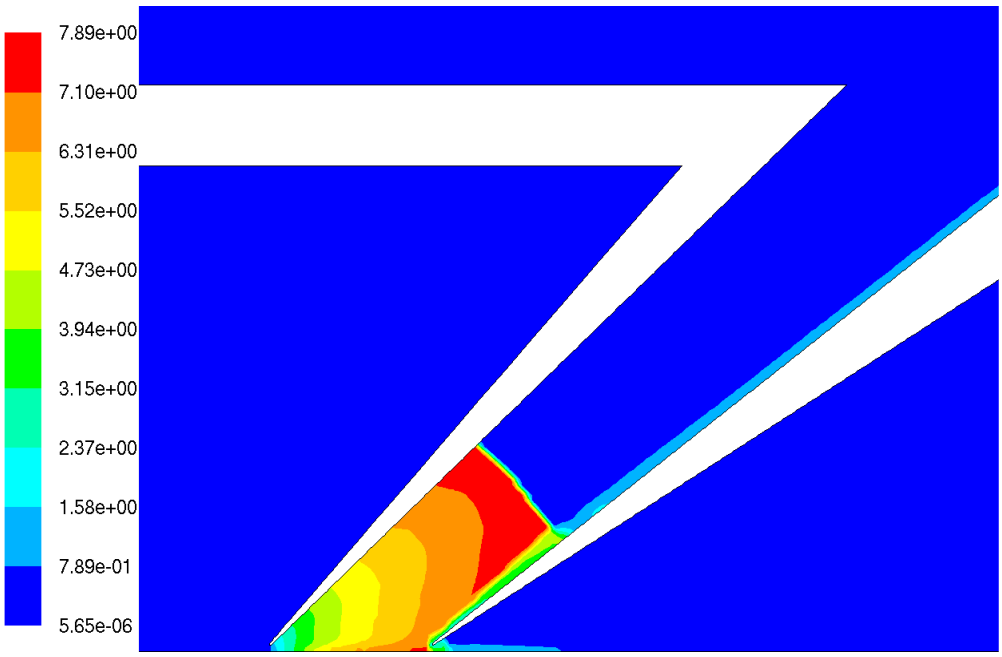


(b)

**Figure 4**: Magnified view of Mach number contours at lower inlet-to-exit pressure ratios: (a) the present analysis; (b) FLUENT result

In order to validate the present results, an axisymmetric inviscid flow solver of the finite-volume-based commercial CFD software FLUENT [11] was used at the same pressure ratios as those in Figure 3 and 4(a), and the result is presented in Figure 4(b). In the FLUENT simulation, 44152 unstructured mesh elements were used in the flow domain, with most of them clustered in the regions where the large changes of Mach numbers are observed in Figure 4(b). Explicit time-marching of the unsteady Euler equation was performed using a first-order upwind scheme, and the dynamic grid adaptation technique was implemented after the solution settled down reasonably well. It is observed that the upper shock in the first vacuum chamber is nearly at the same location and of roughly the same strength, judging from the maximum Mach number within the expansion region. The difference in shock structure is the absence of a shock in the second vacuum chamber in the FLUENT result. This and other discrepancies may be attributed to a different amount of numerical viscosity inherent in the two simulations. Numerical viscosity is an intrinsic feature of any inviscid flow solver, and it must be present to some degree to obtain numerically stable solutions. The greater the numerical viscosity, the more stable will be the computation, although strong flow gradients will tend to wash out. An inviscid flow solver with low numerical viscosity will better preserve strong flow gradients, although in the vicinity of shocks spurious oscillations may occur, which can occasionally destabilize the computation.

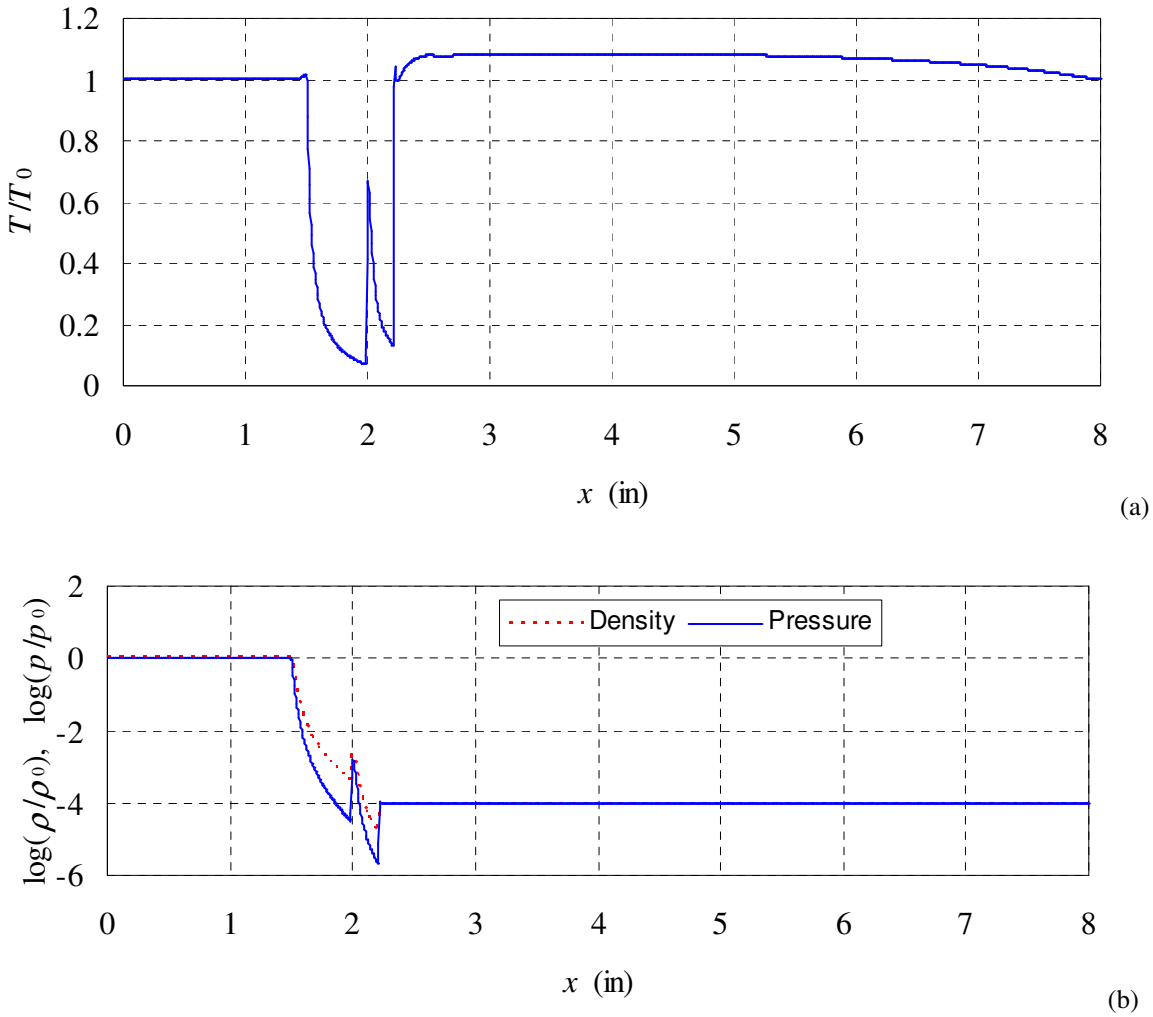


**Figure 5**: Flow properties along the axis at lower inlet-to-exit pressure ratios

Since the flow at both inlet and exit is of very low Mach number, and since the stagnation temperature does not change across the shock waves, the static temperatures at inlet and exit must be about the same. This is observed in the temperature distribution along the axis, shown in Figure 5(a). Note that the strongest shock identified in Figure

4(a) does not appear in Figure 5(a) since it does not cross the centerline axis, however the other two shocks are clearly visible by the two nearly vertical lines. The slight temperature overshoot is because of incomplete convergence of the temperature field. Inviscid flow has no effective heat transfer mechanism, and thus the full convergence of the temperature field requires an overwhelmingly large amount of computation time. Pressure and density are presented in Figure 5(b), which is another plot that also focuses on the variation of properties along the axis. Since both the pressure and density change by several orders of magnitude, a logarithmic scale was used in Figure 5(b). The solid line indicates $\log(p/p_0)$ and the dotted line is $\log(\rho/\rho_0)$. The two curves overlap for small values of $x$ less than approximately 1.5 inches and also for large values greater than approximately 2.5 inches. Most importantly, it was observed in the computation that all three shocks shown in Figures 3, 4, and 5 are fixed in space and hence the entire flow reaches a steady state.

Figure 6 shows the magnified view of Mach number contours in the first vacuum chamber and its vicinity near the axis at higher inlet-to-exit pressure ratios of $p_0/p_1$ = 1E+4, $p_0/p_2$ = 1E+5, and $T_0$ = 295 K. The fluid is nitrogen in this computation, and the gas constant and the specific heat ratio are $R$ = 297 J/(kg·K) and $\gamma$ = 1.4. The overall flow field is similar to that of the lower pressure ratio case although the shocks are stronger due to the increased pressure difference between the high pressure and vacuum chambers. As a result, the upper shock within the first vacuum chamber does not reach a fixed location but periodically moves out of the nozzle, dissipates within the upper chamber, and then collapses back into the nozzle. Even though this periodic movement is very pronounced, there seems to be little influence on the flow properties along the optical axis, which remain nearly constant over time. Only a slight back and forth movement of the third shock, located within the second vacuum chamber, was observed with a periodicity comparable to the first chamber shock.

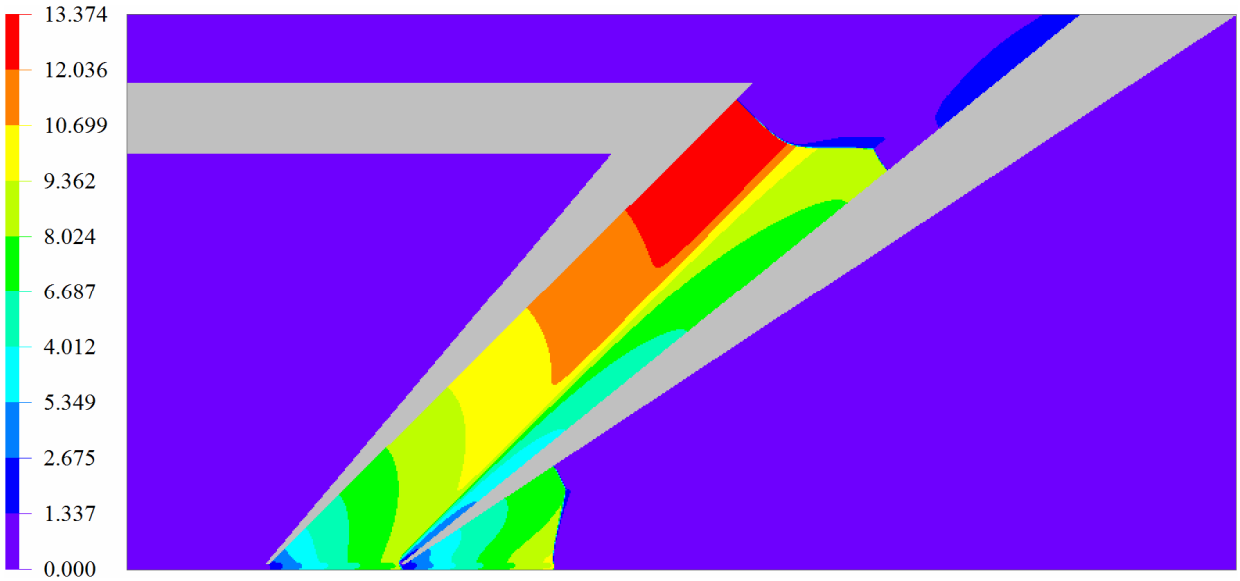


**Figure 6**: Magnified view of Mach number contours at higher pressure ratios

One may argue that as long as there is at least an order of magnitude pressure drop between successive chambers, the flow will go through expansion and compression cycles, with locally supersonic flow followed by shock waves as described above. Whether the flow is ultimately steady or unsteady, after its initial transient has died out, depends on the expansion or area ratio of each nozzle and the pressure drop across it. Although it is possible to design a nozzle through smooth contouring, which would create a jet of supersonic exit flow, such geometries are to be avoided. A flow should be of low Mach number once it exits a vacuum chamber, such that pressure, density and temperature are constant until the electrons reach the analyzer. Simulation attempts using FLUENT were not successful at these higher pressure ratios because of numerical instability. As mentioned earlier, this may be attributed to the low numerical viscosity of the inviscid flow solver of FLUENT.

## IV. Conclusion

Numerical solutions of the supersonic flow field in the vacuum chambers of a high-pressure-ratio photo-emission gas spectrometer were obtained with the use of Van Leer's inviscid flux vector splitting method, and the results showed good agreement with those obtained by the commercial CFD software FLUENT. Shock waves, both stationary and moving, were well resolved at all pressure ratios. In both the present analysis and the implementation of the FLUENT software, it was difficult to achieve a complete convergence of the temperature field. Since there is no effective heat transfer mechanism in an inviscid flow, the temperature gradients within a stagnation region can take orders of magnitude longer to settle down compared to the simulation time scales needed for pressure and density convergence.

The uniform Cartesian mesh with cut cells used in the present analysis provides significant advantages by allowing a simple and fast geometry setup and mesh generation. This greatly reduced the amount of effort and time in automating the design studies of various geometries. Numerous other chamber geometries were tested over the course of the investigation, yet these cases were not included here for the sake of brevity.

As the flow approaches the free molecular regime, a direct simulation Monte Carlo method can produce more accurate results than the present analysis, which relies on the continuum assumption. Alternatively, studies could be performed for spectrometers that operate at higher overall pressures so that the continuum hypothesis of the flow can always be guaranteed.

## Acknowledgement

Partial support for this work was provided by Berkeley National Laboratory through Subcontract No. 6713807. The authors would like to thank Dr. Zahid Hussain and Dr. Gennadi Lebedev for this opportunity.

## References

[1] Wikipedia, The Free Encyclopedia: *Photoemission Spectroscopy*. http://en.wikipedia.org/wiki/Photoemission_spectroscopy.
[2] Wikipedia, The Free Encyclopedia: *Photo Electric Effect.* http://en.wikipedia.org/wiki/Photoelectric_effect.
[3] D. Frank Ogletree, Hendrik Bluhm, Gennadi Lebedev, Charles S. Fadley, Zahid Hussain, Miquel Salmeron. *A differentially pumped electrostatic lens system for photoemission studies in the millibar range*. American Institute of Physics, Review of Scientific Instruments, Volume 73, Number 11, November 2002, 3872-3877.
[4] *MicroCFD* ® Virtual Wind Tunnel. CFD shareware developed by MicroCFD.com. http://www.microcfd.com/software.htm.
[5] Meng-Sing Liou, Bram Van Leer, Jian-Shun Shuen. *Splitting of Inviscid Fluxes for Real Gases*. NASA Technical Memorandum 100856, April 1988.
[6] Alina Alexeenko. *Modeling of Microscale Gas Flows using the Direct Simulation Monte Carlo Method*. Dissertation in Aerospace Engineering, Penn State University, October 2003.
[7] Walter Vincenti, Charles Kruger. *Introduction to Physical Gas Dynamics*. Krieger Publishing Company, Florida, 1986.
[8] John David Anderson. *Hypersonic and High Temperature Gas Dynamics*. McGraw-Hill, 1989, 20-23 (*Low-Density Flow*).
[9] *Visual DSMC*. DSMC shareware developed by GAB (Graeme A. Bird) Consulting. http://www.gab.com.au/.
[10] Graeme A. Bird. *Molecular Gas Dynamics and the Direct Simulation of Gas Flows*. Oxford University Press, 1994.
[11] FLUENT ®. CFD software developed by FLUENT, Inc, (acquired by ANSYS, Inc). http://www.fluent.com/.